

Bulk-Boundary Correspondence in 2D Topological Photonics: Analysis and Simulation

Igor Tsukerman

*Department of Electrical and Computer Engineering,
The University of Akron, OH 44325-3904*

E-mail: igor@uakron.edu

(Dated: January 7, 2025)

The centerpiece of topological photonics is the bulk-boundary correspondence principle (BBCP), which relates discrete invariants of the Bloch bands to the possible presence of topologically protected interface modes between two periodic heterostructures. In addition to the fundamental significance of BBCP, interface modes are of interest in a variety of applications. In Maxwell's electrodynamics, the BBCP has been rigorously proved for 1D problems, but the 2D case is qualitatively different, because the boundary conditions involve nontrivial Dirichlet-to-Neumann maps rather than scalar impedances as in 1D. The theoretical analysis and numerical examples presented in the paper are consistent with the BBCP. Moreover, the BBCP is closely connected with the positivity of electromagnetic energy density, as has also been shown to be the case in 1D and 1.5D.

I. INTRODUCTION

The main tool of field analysis in periodic structures is propagating Bloch modes, forming a set of bands separated by frequency gaps. Under assumptions (i)–(ii) below, each band can be assigned a discrete *topological invariant* – Zak phase, zero or π , in 1D or an integer Chern number in 2D [1–3]. The topological invariance is with respect to any continuous bandgap-preserving changes of geometric and material parameters of the lattice cell. Throughout the paper, we assume that (i) the lattice cells are mirror-symmetric (Sec. II), and (ii) losses can be neglected, so that non-Hermitian topological photonics [4, 5] remains outside the scope of the paper.

If two different periodic structures abut, there may or may not exist modes, either standing or traveling along the interface boundary and confined to that interface. The centerpiece of topological photonics is the bulk boundary correspondence principle (BBCP), which relates the possible presence of interface modes in a bandgap to the discrete invariants of all Bloch bands below that gap. In addition to its fundamental significance, BBCP has practical applications, since topologically protected modes are of interest in communication, topological lasers, and other areas [2, 6–8].

The BBCP is surprising in several respects. First, note that Bloch bands can be defined and calculated over a single lattice cell under Bloch-periodic boundary conditions (Sec. II); this has nothing to do with material interfaces, where the translational symmetry of an infinite lattice is broken. Thus, conclusions about *boundary* modes are drawn after ignoring the presence of the boundary to begin with; this is puzzling.

Furthermore, the BBCP relates *evanescent* modes within a particular bandgap[9] to *propagating waves at all lower frequencies*. Indeed, the relevant parameter is the *gap* Chern number or *gap* Zak phase – that is, the sum of Chern numbers (Zak phases) over all bands below a given gap. For example, the existence of *evanescent* boundary modes at optical frequencies depends, in some way, on *propagating* waves at radio frequencies, power frequencies, and even on the zero-frequency (static) field. This is perplexing and needs to be understood from both mathematical and physical perspectives.

A short historical note on the status of the BBCP is apposite. The relevant developments span over half a century – from Pancharatnam's work in the 1950s [10] to the quantum Hall effect [11] to the discovery of topological insulators [12], with many advances in between. The findings and conclusions of the elaborate topological theories in condensed matter physics were then translated to electrodynamics [1, 2, 6]. While this translation has been quite productive and has resulted in vigorous research activity over the last two decades, there are significant differences between the equations and boundary conditions of condensed matter physics and electrodynamics. Many topological theories of the former involve tight binding, lattice or finite difference models [13–15]. In the continuous case, there exists sophisticated mathematical work utilizing, among other things, Fredholm index theory for single-particle Schrödinger Hamiltonians [16–18]; it remains to be seen to what extent these studies apply to electromagnetic problems.

The present paper deals exclusively with continuous Maxwell electrodynamics. Over the last ten years, the BBCP was rigorously proved for lossless media in 1D and 1.5D [19–22]. “1.5D” refers to the case where material parameters depend only on the coordinate n normal to the interface; mathematically, the problem can be reduced to one dimension, but the fields and wave vectors may have two components. A central role in the analysis and proof of the BBCP in 1D is played by the Bloch boundary impedance or, alternatively, admittance (the inverses of one another) [19–22]. In 2D, the scalar admittance turns, mathematically, into an infinite dimensional (in the functional-analytic sense) Dirichlet-to-Neumann (DtN) map (Sec. III), which can be expressed, e.g., in the basis of spatial harmonics along the interface.

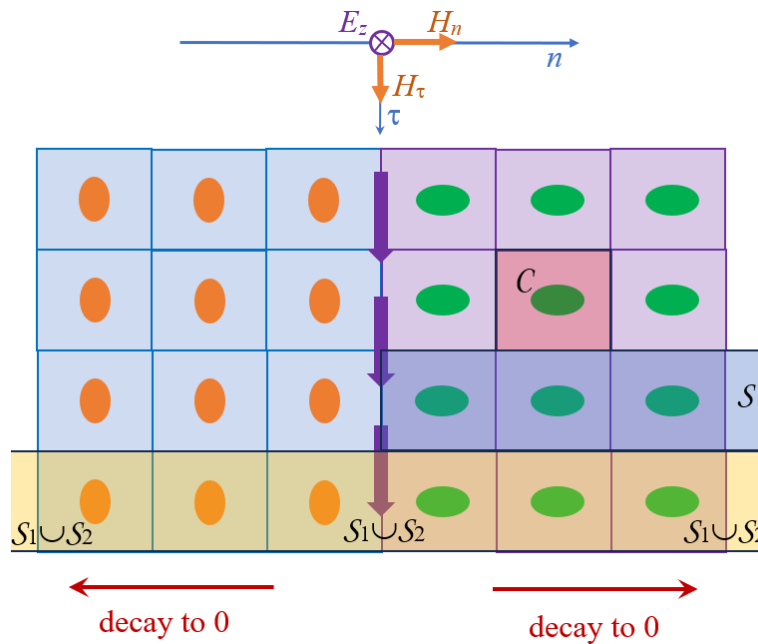


FIG. 1. A schematic illustration of two abutting structures; s mode is assumed. The purple vertical arrows indicate a possible direction of propagation of a boundary mode, if it exists.

The paper is devoted to an analytical, semi-analytical and numerical study of the DtN maps and the respective interface matching conditions. Four interrelated Bloch and Dirichlet problems are formulated in Sec. II. The DtN map for a semi-infinite strip can be defined and computed via a set of evanescent Bloch modes in the lattice cell (Sec. III). Numerical case studies include a combination of gyromagnetic and simple dielectric/magnetic media (Sec. IV).

II. FORMULATION OF FOUR RELATED PROBLEMS

A canonical setup is shown in Fig. 1. In this paper, only rectangular lattices are considered, with cells scaled to $a \times a$ squares for convenience. Each of the two periodic heterostructures fills its respective half-space. A fundamental question is this: Under what conditions do there exist one or more modes evanescent in the normal direction n – either standing waves or traveling in the tangential direction τ along the boundary? Purportedly, the BBCP answers this question; however, as noted in the Introduction, a rigorous proof exists in some cases but, to the best of my knowledge and understanding, not for 2D Maxwell problems.

The main part of the paper focuses on the purest case of topological electrodynamics, whereby losses and frequency dependence (“frequency dispersion”) of material parameters are neglected. The lossy case falls under the umbrella of non-Hermitian photonics [5] and, in 1D, is the subject of Ref. [23]. Accounting for frequency dispersion in my analysis is not conceptually difficult, as demonstrated by the derivation in the Appendix; the relevant techniques have already been worked out in 1D [22] and in 1.5D [24].

For definiteness, we assume the s -mode (one-component electric field $\mathbf{e} = \hat{z}e$ and the respective two-component magnetic field $\mathbf{h} = h_n \hat{n} + h_\tau \hat{\tau}$); analysis for the p -mode is similar. Hats indicate unit vectors; the coordinate system (n, τ, z) is right-handed. The complex amplitudes $\mathbf{e}(n)$ and $\mathbf{h}(n)$ satisfy Maxwell’s equations:

$$\nabla \times \mathbf{e}(n, \tau) = ik\mu(n, \tau) \mathbf{h}(n, \tau), \quad \nabla \times \mathbf{h}(n, \tau) = -ik\epsilon(n, \tau) \mathbf{e}(n, \tau) \quad (1)$$

in the Gaussian system under the $\exp(-i\omega t)$ phasor convention; $k = \omega/c$ is the wave number. For the s mode, the magnetic permeability $\mu(n, \tau)$ may in some cases be anisotropic and represented in the (n, τ) coordinates as a 2×2 matrix (Sec. IV); ϵ is scalar. Eliminating the magnetic field \mathbf{h} from (1), one arrives at the electric field equation:

$$\nabla \cdot (\rho(n, \tau) \nabla e(n, \tau)) + k^2 \epsilon(n, \tau) e(n, \tau) = 0 \quad (2)$$

where ρ is related to the magnetic permeability tensor μ and its inverse ν as

$$\rho = \begin{pmatrix} \rho_{nn} & \rho_{n\tau} \\ \rho_{\tau n} & \rho_{\tau\tau} \end{pmatrix} = \begin{pmatrix} \nu_{\tau\tau} & -\nu_{\tau n} \\ -\nu_{n\tau} & \nu_{nn} \end{pmatrix}; \quad \nu = \begin{pmatrix} \nu_{nn} & \nu_{n\tau} \\ \nu_{\tau n} & \nu_{\tau\tau} \end{pmatrix} = \mu^{-1} \quad (3)$$

For a given periodic heterostructure on a rectangular lattice, the material parameters satisfy

$$\epsilon(n + m_n a, \tau + m_\tau a) = \epsilon(n, \tau); \quad \mu(n + m_n a, \tau + m_\tau a) = \mu(n, \tau); \quad (m_n, m_\tau) \in \mathbb{Z}^2 \quad (4)$$

as long as both points $(n + m_n a, \tau + m_\tau a)$ and (n, τ) lie within that structure. For brevity, we assume that the medium right next to the interface boundary is nonmagnetic: $\rho(n = 0, \tau) = 1$. The lattice cells are assumed to be mirror-symmetric with respect to n :

$$\epsilon(a - n, \tau) = \epsilon(n, \tau); \quad \mu(a - n, \tau) = \mu(n, \tau) \quad (5)$$

Note that if the structure occupies the whole space, mirror symmetry and periodicity imply that the material parameters are even functions of n :

$$\epsilon(-n, \tau) \stackrel{\text{periodicity}}{=} \epsilon(a - n, \tau) \stackrel{\text{symmetry}}{=} \epsilon(n, \tau) \quad (6)$$

and the same for μ . The overall setup is schematically represented in Fig. 1. The boundary modes satisfy Maxwell's equations (1), (2), with Bloch boundary conditions (8) on the τ sides of a single semi-infinite strip $S = [0, \infty] \times [-a/2, a/2]$, and decaying to zero in the normal direction on both sides.

Four interrelated auxiliary problems play an important role in the analysis. One is the Bloch problem over a single lattice cell $\Omega_C : 0 \leq n \leq a; -a/2 \leq \tau \leq a/2$:

$$e(n + a, \tau) = \exp(i\beta a) e(n, \tau); \quad \partial_n e(n + a, \tau) = \exp(iqa) \partial_n e(n, \tau) \quad (7)$$

$$e(n, \tau + a) = \exp(i\beta a) e(n, \tau); \quad \partial_\tau e(n, \tau + a) = \exp(i\beta a) \partial_\tau e(n, \tau) \quad (8)$$

Different symbols for the Bloch wavenumbers q (in the n direction) and β (in the τ direction) are used because they play different roles in the physical setup and mathematical analysis. In particular, of our primary interest are modes propagating in the τ direction with a real β and evanescent in the n direction, with a purely imaginary q . The Maxwell cell problem (1) with Bloch boundary conditions (7), (8) has three eigenparameters: k , β and q . It will be convenient to treat the first two of them as given and the third one, q , as an unknown. Some expressions simplify if the τ -periodic factor $\tilde{e}(n, \tau)$ is used instead of $e(n, \tau)$:

$$e(n, \tau) = \tilde{e}(n, \tau) \exp(i\beta\tau); \quad \tilde{e}(n, a/2) = \tilde{e}(n, -a/2) \quad (9)$$

The second and third auxiliary problems (Sec. III) have to do with the DtN operators on the boundary of a single lattice cell and a semi-infinite strip $S = [0, \infty) \times [-a/2, a/2]$, respectively; the strip is composed of an infinite number of cells. Formally, the boundary conditions for S are (8) on the $\tau = \pm a/2$ sides and

$$e(n, \tau) \rightarrow 0 \text{ as } n \rightarrow \infty; \quad \partial_n e(n, \tau) \rightarrow 0 \text{ as } n \rightarrow \infty \quad (10)$$

uniformly with respect to n, τ . One complication is that the standard radiation conditions at $n \rightarrow \infty$ do not apply, since there is no free space in this setup. Instead, the condition at infinity can be defined via a set of evanescent Bloch modes in a lattice cell:

$$e(n, \tau) = \sum_m c_m e_m(n, \tau); \quad \sum_m |c_m|^2 = 1 \quad (11)$$

$$e_m(n, \tau) \text{ satisfy (1), (7), (8), with } q = q_m, \quad m = 1, 2, \dots; \quad \int_C (e_m^2 + |\nabla e_m|^2) dC = 1 \quad (12)$$

Strictly speaking, (12) for each m defines a family of modes which differ by an arbitrary phase factor $\exp(i\phi)$, $\phi \in \mathbb{R}$; let e_m denote one representative of this family.

Finally, solutions over the abutting semi-infinite strips $S_{1,2}$ must be matched at the interface through Maxwell's boundary conditions (Sec. III).

The parity of Bloch modes at the Γ and X points is known to have major implications in 1D, through a direct connection with the nulls and poles of the Bloch boundary impedance (see [21] for details and references). It is proved in [20–22] that impedance monotonically decreases as a function of frequency within any band gap.

In 2D, the situation is qualitatively more involved. Admittance turns into a DtN map, defined below and well known in the theory of partial differential equations and in inverse problems. As shown in the Appendix, the DtN operator is monotone as a function of frequency. This generalization of the monotonicity of 1D impedance is interesting but unfortunately not sufficient to prove the BBCP in 2D mathematically.

III. DIRICHLET-TO-NEUMANN (DTN) OPERATORS: DEFINITION AND COMPUTATION

The main stage of the analysis has to do with the behavior of fields in a single semi-infinite strip $S = (0 \leq n < \infty; |\tau| \leq a/2)$ composed of repeated lattice cells $C = [0, a] \times [-a/2, a/2]$. The electric field satisfies the generalized Helmholtz equation (2), the Bloch boundary condition at $\tau = \pm a/2$, and the decay condition (10) at infinity. The Dirichlet-to-Neumann (DtN) map \mathcal{D} relates the values of e and $\partial_n e$ at the boundary $n = 0$ of S :

$$\partial_n e(0, \tau; k, \beta) = \mathcal{D}(k, \beta) e(0, \tau) \quad (13)$$

Since the n -derivative does not affect the complex exponential $\exp(i\beta\tau)$, one can easily alternate between e and \tilde{e} (9) in the expressions below. To simplify these expressions slightly, and without much loss of generality, we shall assume that the material immediately adjacent to the interface $n = 0$ is nonmagnetic; otherwise the magnetic permeability at $n = 0$ would appear in the matching conditions. Function arguments are omitted whenever this should not cause confusion.

Our starting point is the computation of the DtN operator for the wave equation (2) in a single lattice cell C . The boundary conditions are

$$\tilde{e}(n, -a/2) = \tilde{e}(n, a/2); \quad \tilde{e}(0, \tau) = \tilde{f}_0(\tau); \quad \tilde{e}(a, \tau) = \tilde{f}_a(\tau) \quad (14)$$

where \tilde{f}_0, \tilde{f}_a are given τ -periodic functions, which can be conveniently represented in the Fourier basis $\psi_m(\tau) = \exp(2\pi i m \tau / a)$, $m = 0, \pm 1, \dots$. This basis is theoretically infinite but can be truncated to a finite one in practical computation. The normal derivatives $\partial_n \tilde{e}$ can also be represented in the same Fourier basis. Using the subscripts ‘l’ and ‘r’ as shorthand for the “left” ($n = 0$) and “right” ($n = a$) edges of the lattice cell C , one can write the DtN map (either exact or approximate) in block form:

$$\partial_n \begin{pmatrix} e_l \\ e_r \end{pmatrix} = \begin{pmatrix} \mathcal{D}_{ll}^C & \mathcal{D}_{lr}^C \\ \mathcal{D}_{rl}^C & \mathcal{D}_{rr}^C \end{pmatrix} \begin{pmatrix} e_l \\ e_r \end{pmatrix} \quad (15)$$

where the superscript ‘C’ refers to the DtN map for the lattice cell. As an alternative to well-known methods of computing Bloch modes, one can, as first proposed in [25, 26], consider (15) in conjunction with the Bloch conditions in the normal direction:

$$e_r = \lambda_B e_l; \quad \partial_n e_r = \lambda_B \partial_n e_l \quad (16)$$

One advantage of the DtN approach is that it generalizes in a natural way to the computation of eigenmodes in a semi-infinite strip and, ultimately, to interface modes between two periodic structures. Elimination of $\partial_n e_r$ from (15), (16) leads to the following quadratic eigenproblem:

$$[\lambda_B^2 \mathcal{D}_{lr}^C + \lambda_B (\mathcal{D}_{ll}^C - \mathcal{D}_{rr}^C) - \mathcal{D}_{rl}^C] e_l = 0 \quad (17)$$

In [25, 26], analytical solutions for cylindrical inclusions and collocation on the lattice cell boundary are employed. In the present paper, the finite element method (FEM) is used to solve $2(2M + 1)$ Dirichlet problems (14) in the Fourier basis $\{\tilde{\psi}_m(\tau)\}$ limited to order $m = -M, \dots, M$. One then obtains a set of $2M + 1$ Bloch modes – propagating for $|\lambda_{B,m}| = 1$ and exponential otherwise. The *decaying* eigenmodes are then used to construct the DtN operator for the *semi-infinite strip* S . This extension of the DtN-Bloch method [25, 26] was previously proposed and applied to bound states in the continuum at the surface of a photonic crystal in Ref. [27], where further numerical details pertaining to this idea can be found.

The DtN operator can be converted, by a linear transformation, from this evanescent basis to the Fourier basis $\{\tilde{\psi}_m(\tau)\}$ along the boundary $n = 0$, $-a/2 \leq \tau \leq a/2$. The numerical details are not central in the present paper and are omitted. But two main advantages of the FEM-based approach are worth noting: (a) applicability to any composition of the lattice cell, and (b) computational efficiency [28].

With the above definitions in place, we can now turn to the boundary conditions at the interface $n = 0$ between the two heterostructures. In 1D, these conditions simply amount to impedance (or admittance) matching. A 2D generalization of these conditions is

$$\text{Null}(\mathcal{D}_1 + \mathcal{D}_2) \neq \emptyset \quad (18)$$

Our convention is to treat the two structures on an equal footing, the normal directions in both cases being *into* the respective domain – hence the plus sign in the expression. The null space, if not empty, contains the boundary value (or values) $e(0, \tau)$ of the possible mode(s) in a chosen basis.

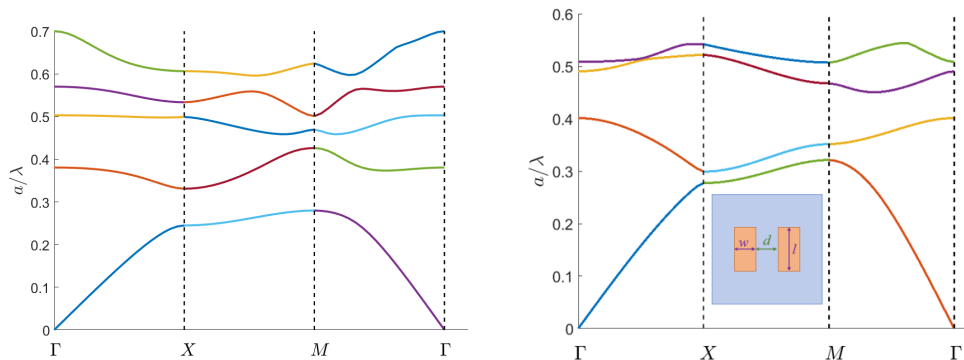


FIG. 2. Band diagrams for a gyromagnetic (left) and simple dielectric/magnetic structures (right). Parameters are specified in the text.

IV. NUMERICAL EXAMPLES

The purpose of the numerical simulations in this section is to investigate the canonical setup: gyromagnetic structures coupled with simple dielectrics/magnetics [2, 6, 29]. Due to the presence of gyromagnetic materials such as YiG, the time reversal symmetry is broken, and some of the relevant topological invariants – the Chern numbers [2, 3, 6, 7] – may be nonzero.

In the simulations reported below, the cell size a of both abutting structures has for convenience been normalized to unity, and the parameters were adjusted to ensure an overlap between the bandgaps of the two heterostructures under investigation. Namely, the permittivity of the gyromagnetic cylinders in the first periodic structure is $\epsilon_{\text{cyl}} = 20$, the host medium has $\epsilon_{\text{host}} = 2$, and the permeability tensor μ has, as in [2, 6, 29], $\mu_{nn} = \mu_{\tau\tau} = 14$ on the diagonal and $\mu_{n\tau} = -\mu_{\tau n} = 12.4i$ off the diagonal. The lattice cell of the second structure contains two rectangular bars $0.2a \times 0.4a$ separated by a $0.2a$ gap (Fig. 2, inset), in an otherwise empty cell. The physical parameters of the bars are $\epsilon_{\text{bar}} = 6$, $\mu_{\text{bar}} = 6$. Then there exists an overlap in the band gaps of the two structures around the normalized frequency $a/\lambda \sim 0.42$; see the band diagrams in Fig. 2.

The simulations were carried out using FE analysis with first order triangular elements; the typical number of elements was on the order of 5,000, although multiple simulations with finer and coarser meshes were also performed to verify convergence. The DtN map for each of the two structures was computed in the basis of Fourier harmonics as described in Sec. III.

In light of the boundary condition (18), of principal interest is the minimum singular value $\sigma_{\min}(\mathcal{D}_1 + \mathcal{D}_2)$. Fig. 3 demonstrates a sharp drop in σ_{\min} at a particular frequency ($a/\lambda \sim 0.42$) within the overlap between the two band gaps. This sharp drop can be contrasted with the smooth variation of the minimum singular values of the two DtN operators separately (Fig. 3), which indicates that a qualitative change occurs when two structures are put together and share a common interface. The maximum order of spatial harmonics is $M = 4$, so that the total number of harmonics between $-M$ and M is nine. Very similar results were obtained with $M = 3$ and $M = 5$. The mode corresponding to $\sigma_{\min}(\mathcal{D}_1 + \mathcal{D}_2)$ for $\beta = 0$ is illustrated in Fig. 3, right.

The visual appearance of the modes for the tangential wavenumber $\beta = 0$ and $\beta \neq 0$ is similar, as long as a bandgap overlap exists. As an example, cf. surface plots of the real part of the electric field in Fig. 3, right ($\beta = 0$) and Fig. 4, left ($\beta = \pi/6$).

The dispersion curve for the interface mode, shown in Fig. 4, right, illustrates an underappreciated point. The difference of the gap Chern numbers $|C_1 - C_2|$ of the respective structures is equal *not* to the total number of boundary modes but, rather, to the “net current” (a.k.a. “spectral flow” in electronic structure theory) – the *difference* between the number of modes traveling in one direction and the other [30, p. 5], [31]. The Chern numbers of the gyromagnetic structure are calculated as in [29, 32] and happen to be zero for the first two bands. Hence the Chern number for the second *gap* (around $a/\lambda \sim 0.42$), which by definition is equal to the sum of the two underlying *band* Chern numbers, is also zero. The dispersion curve of Fig. 4 indicates the presence of *two* modes traveling in the opposite directions, implying that the “net flow” at the interface is zero; this is consistent with the gap Chern number being zero.

In addition to the geometric setup with the two bars, multiple simulations with *cylindrical* inclusions in the dielectric/magnetic structure were performed; parameters were chosen to produce approximately the same bandgap overlap at $a/\lambda \sim 0.42$. The results in all these cases were similar not only qualitatively but quantitatively, and therefore are not reported here.

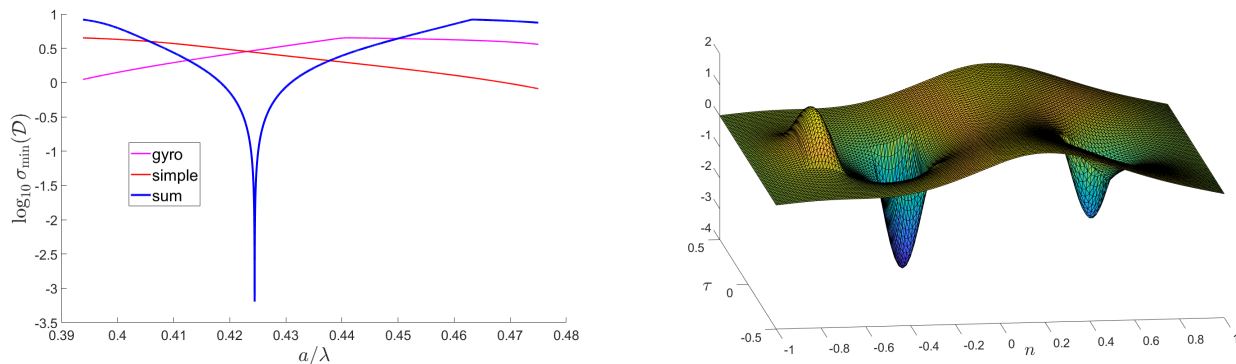


FIG. 3. Left: The minimum singular value $\sigma_{\min}(\mathcal{D}_1 + \mathcal{D}_2)$ exhibits a sharp drop at a particular frequency within a gap, in contrast with the smooth variation of the individual minimum singular values of the two DtN operators. Right: the real part of the electric field of the mode corresponding to $\sigma_{\min}(\mathcal{D}_1 + \mathcal{D}_2)$. The simple and gyromagnetic media occupy the half-spaces $n \leq 0$ and $n \geq 0$, respectively. $\beta = 0$; other parameters are specified in the text.

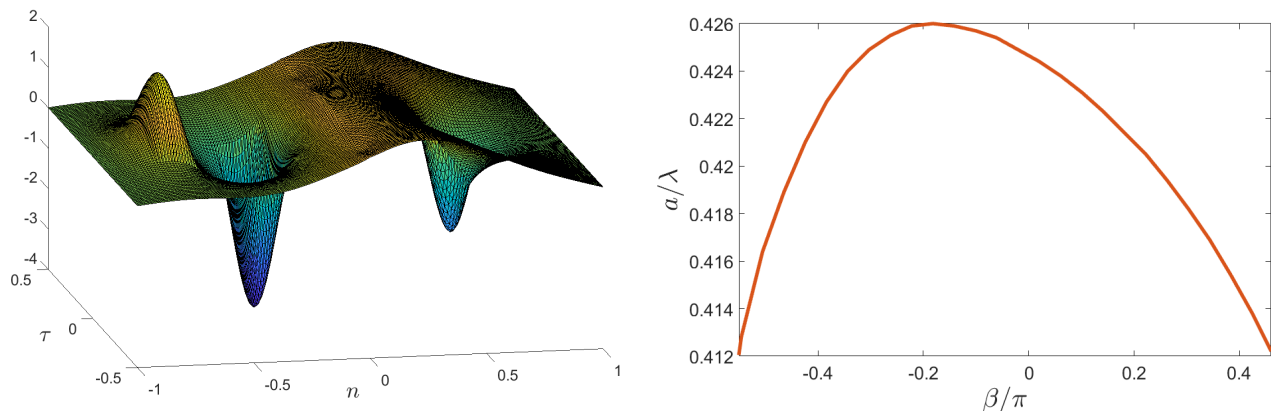


FIG. 4. Left: same as in Fig. 3, right, but for $\beta = \pi/6$. Right: the dispersion curve for the evanescent edge mode. Parameters are specified in the text.

V. DISCUSSION AND CONCLUSION

The objective of the paper is to examine, analytically and numerically, the validity of the BBCP for problems of 2D Maxwell’s electrodynamics. The study is limited to rectangular lattices, although some of the methods and considerations are applicable to hexagonal lattices (“valley photonics” and the “photonic spin Hall effect” [7, 8]). Other topological issues, such as waveguides [33, 34] and non-Hermitian topological photonics are outside the scope of the paper.

The BBCP has been mathematically proven for a range of cases in 1D and 1.5D. The qualitative difference with 2D is that the boundary admittance, a scalar quantity in 1D, turns into an infinite-dimensional DtN map. In the paper, this map is defined and computed for semi-infinite strips in the basis of spatial harmonics along the boundary. A very similar approach was proposed in [27] for the computation of bound states in the continuum at a photonic crystal/air interface.

A sufficient and necessary condition for the existence of an interface mode within an overlap of the bandgaps is for the sum of the DtN maps of the two abutting structures to be singular. This is detected numerically as a sharp minimum of the singular value of the sum of the DtN operators in a basis of spatial harmonics.

From a purely mathematical standpoint, the numerical results cannot be fully conclusive, as the singularity of an infinite-dimensional operator cannot generally be verified exactly – not to mention that numerical studies are by necessity limited in scope and lack generality. But from a physical perspective, results presented in this paper are persuasive in several important respects. First, they give a strong indication that the BBCP is indeed exact in 2D Maxwell’s electrodynamics, despite the qualitative differences with 1D and with discrete lattice models. Second, the numerical simulations illustrate the fact that the difference in the gap Chern numbers of the two periodic structures is equal *not* to the total number of interface modes but rather to the “net current” of these modes. Third, the analysis

suggests a connection between the BBCP and the positivity of electromagnetic energy density.

VI. ACKNOWLEDGMENT

Communication with Hai Zhang, Che Ting Chan, Didier Felbacq, Ya Yan Lu, Ralf Hiptmair and Vadim Markel is very gratefully acknowledged.

APPENDIX: MONOTONICITY OF THE DTN OPERATOR IN A GAP

The 2D analysis consists of three main steps: 1) differentiate the wave equation (2) with respect to $s = k^2 = (\omega/c)^2$, leading to an equation for the derivative $g = \partial_s e$; 2) inner-multiply this equation for g with e and integrate by parts, to arrive at the boundary values of the fields; 3) algebraically simplify the result to obtain a relationship for the DtN operator. For 1D problems, this plan was pioneered in [20], with some simplification given in [24].

In 1D, the boundary admittance (inverse of impedance) is a scalar; in 2D, it turns into the Dirichlet-to-Neumann (DtN) operator $\mathcal{D}(s)$:

$$\partial_n e(0, \tau; s) = \mathcal{D}(s) e(0, \tau; s) \quad (19)$$

This operator is self-adjoint in the space of functions satisfying the Bloch conditions at $\tau = \pm a/2$ and decaying at $n \rightarrow \infty$. This can be shown by the standard integration-by-parts argument, keeping in mind that the functions are complex valued. Indeed, let $u = u(n, \tau; s)$, $v = v(n, \tau; s)$ be two arbitrary solutions of problem (1), (8), (11) in S . The arguments of the functions will be dropped whenever this does not cause confusion; then

$$0 = (\nabla \cdot (\rho \nabla u) + s \epsilon u, v) \stackrel{\text{Green's id.}}{=} -[\partial_n u, v] - (\rho \nabla u, \nabla v) + s(\epsilon u, v) \quad (20)$$

$$0 = (\nabla \cdot (\rho \nabla v) + s \epsilon v, u) \stackrel{\text{Green's id.}}{=} -[\partial_n v, u] - (\rho \nabla v, \nabla u) + s(\epsilon v, u) \quad (21)$$

where the inner products over the strip S and its boundary $n = 0$ are defined as follows:

$$(u, v) = \int_S u v^* dS; \quad [u, v] = \int_{-a/2}^{a/2} u(0, \tau) v^*(0, \tau) d\tau \quad (22)$$

The negative sign of the boundary terms in (20), (21) reflect the fact that the n coordinate is directed *into* the domain. In the process of integration by parts, the contribution at $n \rightarrow \infty$ vanishes, and the boundary terms at $\tau = \pm a/2$ cancel out due to the conjugate exponentials $\exp(\pm i\beta a/2)$. Noting that ϵ is real and ρ is Hermitian by our assumptions, we obtain after subtracting (20) from the conjugate of (21):

$$[\partial_n u, v] - [u, \partial_n v] = 0 \quad \Leftrightarrow \quad [\mathcal{D}u, v] = [u, \mathcal{D}v] \quad (23)$$

We now proceed to the main part of the analysis. The governing equation (2) for e , with $s = k^2$, is

$$\nabla \cdot (\rho \nabla e) + s \epsilon e = 0 \quad (24)$$

Differentiation of (24) and of (19) with respect to s yields, respectively,

$$\nabla \cdot (\rho \nabla g) + w e + s \epsilon g = 0 \quad (25)$$

$$\partial_n g(0, \tau; s) = [\partial_s \mathcal{D}(s)] e(0, \tau; s) + \mathcal{D}(s) g(0, \tau; s) \quad (26)$$

where the following notation for the s -derivatives has been used:

$$g(n, \tau; s) = \partial_s e(n, \tau; s); \quad w(n, \tau; s) = \partial_s [s \epsilon(n, \tau; s)] \quad (27)$$

Inner-multiplying (25) with e we get, after complex conjugation, and keeping in mind that ϵ and w are real under our assumptions,

$$(\nabla \cdot (\rho \nabla g), e)^* + (w e, e) + s(\epsilon e, g) = 0 \quad (28)$$

The last term can be transformed due to (24):

$$(\nabla \cdot (\rho \nabla g), e)^* + (we, e) - (\nabla \cdot (\rho \nabla e), g) = 0 \quad (29)$$

Applying Green's identity to the two divergence terms, recalling that $\rho(0, \tau) = 1$ by assumption and n is directed inward, one obtains

$$[\partial_n e, g] - [e, \partial_n g] + (we, e) = 0 \quad (30)$$

Note parenthetically that in general $\partial_n g \neq \mathcal{D}g$, since g is not a solution of the wave equation; thus, the inner products in (30) do not cancel despite the Hermiticity of \mathcal{D} . Of the boundary terms, only the $n = 0$ integrals have survived in (30); all other contributions vanish due to the Bloch periodicity of functions in the τ direction and their decay at infinity.

We now substitute into (30) expressions (19) for $\partial_n e(0, \tau; s)$ and (26) for $\partial_n g(0, \tau; s)$:

$$[\mathcal{D}e, g] - [e, (\partial_s \mathcal{D})e + \mathcal{D}g] + (we, e) = 0 \quad (31)$$

The two terms containing \mathcal{D} in (31) cancel out because the DtN operator is self-adjoint, and this equation simplifies:

$$[(\partial_s \mathcal{D})e, e] = (we, e) \quad (32)$$

The right hand side of this relation is physically significant: the quantity $w(\omega) = \partial_s(s\epsilon(s)) = \epsilon(\omega) + \frac{1}{2}\omega \partial_\omega \epsilon(\omega)$ is closely related to the Brillouin-Landau-Lifshitz definition of electromagnetic energy density $w_{\text{BLL}} = \partial_\omega(\omega\epsilon(\omega)) = \epsilon(\omega) + \omega \partial_\omega \epsilon(\omega)$ [35, p. 92], [36, §80, §84], which must be positive in any physical medium; see [24] for a few additional algebraic details.

Since the boundary trace $e(0, \tau; s)$ in (32) can be arbitrary, we have arrived at the following generalization of the monotonicity of impedance. For any physically realizable structures (with a positive density of electromagnetic energy), the s -derivative of the DtN operator is positive definite. It follows that \mathcal{D} is monotonically increasing as an operator in the following sense:

$$\forall s_1 < s_2, \quad \mathcal{D}(s_1) < \mathcal{D}(s_2) \Leftrightarrow (\mathcal{D}(s_1)x, x) < (\mathcal{D}(s_2)x, x), \quad \forall x \in \text{dom } \mathcal{D}, \quad x \neq 0 \quad (33)$$

This is true because integrals of positive definite operators are themselves positive definite:

$$\mathcal{D}(s_2) = \mathcal{D}(s_1) + \int_{s_1}^{s_2} \partial_s \mathcal{D}(s) ds > \mathcal{D}(s_1) \quad \therefore \quad (34)$$

- [1] F. D. M. Haldane and S. Raghu, Possible realization of directional optical waveguides in photonic crystals with broken time-reversal symmetry, *Phys. Rev. Lett.* **100**, 013904 (2008).
- [2] Z. Wang, Y. D. Chong, J. D. Joannopoulos, and M. Soljačić, Reflection-free one-way edge modes in a gyromagnetic photonic crystal, *Phys. Rev. Lett.* **100**, 013905 (2008).
- [3] D. Vanderbilt, *Berry Phases in Electronic Structure Theory: Electric Polarization, Orbital Magnetization and Topological Insulators* (Cambridge University Press, 2018).
- [4] A. Banerjee, R. Sarkar, S. Dey, and A. Narayan, Non-Hermitian topological phases: principles and prospects, *Journal of Physics: Condensed Matter* **35**, 333001 (2023).
- [5] Q. Yan, B. Zhao, R. Zhou, R. Ma, Q. Lyu, S. Chu, X. Hu, and Q. Gong, Advances and applications on non-Hermitian topological photonics, *Nanophotonics* **12**, 2247 (2023).
- [6] Z. Wang, Y. Chong, J. Joannopoulos, and M. Soljačić, Observation of unidirectional backscattering-immune topological electromagnetic states, *Nature* **461**, 772 (2009).
- [7] A. B. Khanikaev and G. Shvets, Two-dimensional topological photonics, *Nature Photonics* **11**, 763 (2017).
- [8] H. Xue, Y. Yang, and B. Zhang, Topological valley photonics: Physics and device applications, *Advanced Photonics Research* **2**, 2100013 (2021).
- [9] More precisely, within a frequency overlap of the bandgaps of the two adjacent heterostructures.
- [10] S. Pancharatnam, Generalized theory of interference, and its applications. Part I. Coherent pencils, *Proc. Indian Acad. Sci. A.* **44**, 247 (1956).
- [11] K. v. Klitzing, G. Dorda, and M. Pepper, New method for high-accuracy determination of the fine-structure constant based on quantized hall resistance, *Phys. Rev. Lett.* **45**, 494 (1980).
- [12] M. Z. Hasan and C. L. Kane, Colloquium: Topological insulators, *Rev. Mod. Phys.* **82**, 3045 (2010).
- [13] Y. Hatsugai, Chern number and edge states in the integer quantum Hall effect, *Phys. Rev. Lett.* **71**, 3697 (1993).

- [14] Y. Hatsugai, Edge states in the integer quantum Hall effect and the Riemann surface of the Bloch function, *Phys. Rev. B* **48**, 11851 (1993).
- [15] E. Prodan and H. Schulz-Baldes, *Bulk and Boundary Invariants for Complex Topological Insulators* (Springer International Publishing, Switzerland, 2016).
- [16] P. Elbau and G. M. Graf, Equality of bulk and edge Hall conductance revisited, *Communications in Mathematical Physics* **229**, 415 (2002).
- [17] J. Kellendonk and H. Schulz-Baldes, Quantization of edge currents for continuous magnetic operators, *Journal of Functional Analysis* **209**, 388 (2004).
- [18] A. Drouot, Microlocal analysis of the bulk-edge correspondence, *Communications in Mathematical Physics* **383**, 2069 (2021).
- [19] M. Xiao, Z. Q. Zhang, and C. T. Chan, Surface impedance and bulk band geometric phases in one-dimensional systems, *Phys. Rev. X* **4**, 021017 (2014).
- [20] G. C. Thiang and H. Zhang, Bulk-interface correspondences for one-dimensional topological materials with inversion symmetry, *Proceedings of the Royal Society A* **479**, 20220675 (2023).
- [21] I. Tsukerman and V. A. Markel, Topological features of Bloch impedance, *Europhysics Letters* **144**, 16002 (2023).
- [22] A. Coutant and B. Lombard, Surface impedance and topologically protected interface modes in one-dimensional phononic crystals, *Proc. R. Soc. A* **480** (2024).
- [23] D. Felbacq and E. Rousseau, Characterizing the topological properties of 1d non-Hermitian systems without the Berry–Zak phase, *Annalen der Physik* **536**, 2300321 (2024).
- [24] I. Tsukerman and V. A. Markel, Topology of Bloch impedance: Traveling waves, dispersive media, and electromagnetic energy, *J Opt*, accepted (2025).
- [25] J. Yuan and Y. Y. Lu, Photonic bandgap calculations with Dirichlet-to-Neumann maps, *J Opt Soc Am A* **23**, 3217 (2006).
- [26] Z. Hu and Y. Lu, Improved Dirichlet-to-Neumann map method for modeling extended photonic crystal devices, *Opt Quant Electron* **40**, 921 (2008).
- [27] Z. Hu and Y. Y. Lu, Propagating bound states in the continuum at the surface of a photonic crystal, *J. Opt. Soc. Am. B* **34**, 1878 (2017).
- [28] The computational cost for the eigenproblem (17) is in practice negligible, since the field at the interface is usually smooth and good accuracy can be attained with a small number of Fourier harmonics. At the same time, sparsity of FE matrices is easier to exploit for Dirichlet solvers than for eigensolvers with large matrices.
- [29] R. Zhao, G.-D. Xie, M. L. N. Chen, Z. Lan, Z. Huang, and W. E. I. Sha, First-principle calculation of Chern number in gyrotropic photonic crystals, *Opt. Express* **28**, 4638 (2020).
- [30] X.-P. Liu, Y. Zhou, Y.-F. Wang, and C.-D. Gong, Characterizations of topological superconductors: Chern numbers, edge states and Majorana zero modes, *New Journal of Physics* **19**, 093018 (2017).
- [31] C.-T. Chan, (2024), private communication.
- [32] T. Fukui, Y. Hatsugai, and H. Suzuki, Chern numbers in discretized Brillouin zone: Efficient method of computing (spin) Hall conductances, *Journal of the Physical Society of Japan* **74**, 1674 (2005).
- [33] S. V. Silva, D. E. Fernandes, T. A. Morgado, and M. G. Silveirinha, Topological pumping and Tamm states in photonic systems, *Phys. Rev. B* **105**, 155133 (2022).
- [34] J. Qiu, J. Lin, P. Xie, and H. Zhang, Mathematical theory for the interface mode in a waveguide bifurcated from a Dirac point, arXiv:2304.10843 (2023).
- [35] L. Brillouin, *Wave Propagation and Group Velocity* (Academic Press, 1960).
- [36] L. Landau and E. Lifshitz, *Electrodynamics of Continuous Media* (Oxford; New York: Pergamon, 1984).